



# Experimental investigations of heat generation and microstructure evolution during friction stir processing of SnSbCu alloy

Beata Leszczyńska-Madej<sup>1</sup> · Joanna Hrabia-Wiśnios<sup>2</sup> · Aleksandra Węglowska<sup>3</sup> · Małgorzata Perek-Nowak<sup>1</sup> · Marcin Madej<sup>4</sup>

Received: 20 June 2022 / Revised: 26 August 2022 / Accepted: 6 September 2022 / Published online: 16 September 2022  
© The Author(s) 2022

## Abstract

The paper presents the results of experimental investigations of the heat generation and microstructure evolution during the friction stir processing (FSP) of the SnSb11Cu6 alloy. The Triflute tool was used for modification; the process was carried out using two rotational speeds of the tool: 280 and 560 RPM and a constant linear speed of 355 mm/min. Microstructure studies were performed employing the techniques of light microscopy and scanning electron microscopy along with analysis of the chemical composition of micro-areas. Additionally, the phase composition was investigated by means of the X-ray diffraction method, and electron backscatter diffraction (EBSD) analysis and hardness testing were performed before and after FSP modification. Furthermore, measurements of the temperature directly on the modified surface by means of a thermal imaging camera and the temperature in the modified zone with a thermocouple system were performed. It was proved that using FSP to modify the SnSbCu alloy promotes refinement and homogenization of the microstructure, as well as improvement of the hardness. The hardness of the starting material was 24 HB, and after FSP, the hardness increased and amounted to, respectively, 25 and 27 HB after processing at 280 and 560 RPM. The microstructure in the stir zone is formed by the dynamic recrystallization (DRX) process and consists of almost equiaxed tin-rich matrix grains with a size of approx. 5–30 µm and fine particles of Cu<sub>6</sub>Sn<sub>5</sub> and SnSb phases. The temperature distribution in the FSP zone is not uniform and changes in a gradient manner.

**Keywords** Friction stir processing · SnSbCu alloy · Microstructure · Heat generation · Dynamic recrystallization (DRX)

## 1 Introduction

The method of modifying the surface layer by friction stir processing (FSP) was developed by Mishra et al. [1] based on the basic principles of friction stir welding technology [2, 3]. However, FSP, unlike friction stir welding (FSW),

is used to modify the microstructure in the surface layer of the product, and not to connect metal elements. The process consists in heating and plasticizing the material as a result of friction of the tool equipped with a shoulder, as well as a pin embedded in the material and moving along the modified surface of the element. The movement of the tool causes heating, strong mixing, and compaction of the deformed material.

The knowledge of the influence of the parameters determines better control over FSP, and thus the final microstructure of the processed material. In addition, incorrectly selected process parameters can lead to rapid tool wear, deformation of the modified element, as well as damage to the clamping system. Therefore, it is important to predict, monitor, and control the forces and torque in particular [4]. The tool torque in FSP is influenced by many factors, including those related to: (1) the tool: the angle of inclination, pin geometry, material, shoulder profile, shoulder-to-pin diameter ratio; (2) clamping system:

✉ Beata Leszczyńska-Madej  
bleszcz@agh.edu.pl

<sup>1</sup> Faculty of Non-Ferrous Metals, AGH University of Science and Technology, 30 Mickiewicza Ave., 30-059 Kraków, Poland

<sup>2</sup> LUKASIEWICZ Research Network-Institute of Non-Ferrous Metals, 19 Pilsudskiego Str., 32-050 Skawina, Poland

<sup>3</sup> LUKASIEWICZ Research Network-Welding Institute, 16-18 Błogosławionego Czesława Ave., 44-100 Gliwice, Poland

<sup>4</sup> Faculty of Metals Engineering and Industrial Computer Science, AGH University of Science and Technology, 30 Mickiewicza Ave., 30-059 Kraków, Poland

clamping force, clamping geometry; (3) material: melting point, properties, chemical composition; (4) devices: clamping force, linear speed, rotational speed; (5) cooling system: temperature, efficiency [5].

A too low tool rotational speed, too high traverse speed, or insufficient clamping force can generate insufficient heat due to poor mixing, resulting in poor material compaction and a porous surface. At a low ratio of rotational speed to linear speed, the heat input reduces the refinement of the microstructure and increases the hardness. Increasing the heat generation will result in greater refinement of the microstructure, improving the properties of the material [6]. An increase in the rotational speed of the tool may result in a change in the morphology and an increase in the refinement of the secondary phases, causing a rise in hardness and a reduction in abrasive wear, as evidenced by the results of the research presented by Alidokht et al. [7]. A too high tool rotational speed, too much tool clamping force, or too low a traverse speed can all contribute to excessive material removal, loss of uniformity, and excessive grain growth due to excessive heat.

Another important parameter determining the microstructure and properties of the processed material is the type and shape of the tool. The main purpose of the tool is to heat up the modified material. The plunging of the pin into the material is possible primarily as a result of heating and plasticization of the processed material due to friction arising from contact with the pin. When the shoulder contacts the surface of the modified element, it exerts pressure on the treated surface, concentrates the plasticized material around the pin, generates frictional heat, and causes plastic deformation in a relatively thin layer (directly below the surface of the shoulder). Another function of the tool is to mix and move the material together. Moreover, the rotating tool should prevent the flow of plasticized material outside the processing zone [8].

The research on FSW and material modification by FSP was aimed, among others, at modelling the material flow behaviour, temperature distribution, and microstructure evolution in the process zone. The first work of Shercliff and Colegrove [9] focused only on the temperature distribution during friction welding and its potential influence on the weld microstructure in addition to the kinetics of precipitate formation. Scientists are now trying to model both the complex behaviour of material flow and the temperature characteristics of mixing processes. Węglowski et al. [10] made a significant contribution to expanding the knowledge on issues related to the numerical modelling of thermal processes during FSP treatment. The authors noted that the initially developed thermal models for the FSW process need to be adjusted for FSP, because the range of rotational speeds and linear velocities used in FSP may be wider than in the FSW process. It is worth mentioning that during surface

treatment with the FSP method, the melting point of the modified materials is not exceeded (the temperature in FSP and/or FSW is 70–90% of the melting point of the modified material) [11]. Nevertheless, owing to the fact that both the pin and the tool shoulder are involved in the heat generation process, the temperature distribution in the process zone is uneven. The highest temperature occurs on the upper surface of the modified zone. In the depths of the material, only the pin generates heat, which maintains a lower temperature in the treatment zones distant from the surface. The results presented by Hamilton et al. [11, 12] prove that the temperature profile is oblique towards the advancing side and leading (initial) edge. In addition, the modified area on the advancing side is usually the hotter side of the process zone and is characterised by a higher stress level compared to the retreating side in the modified material [13], which is influenced by the consistent direction of rotation and tool travel on the advancing side, while on the retreating side, these directions are opposite. In the case of a constant linear speed, with the increment in the rotational speed, the temperature distribution becomes more symmetrical, and the point of maximum temperature moves from the advancing side towards the retreating side [12].

The selection of optimal process parameters is a key element to obtain the desired surface quality, microstructure and properties. On the other hand, the wrong combination of parameters results in improper homogeneity of the material, and consequently, low strength and plasticity. The use of the FSP method to modify the microstructure allows its significant refinement. Many examples of grain refinement as a result of FSP modification are cited in the works presented by, among others, Ma et al. [14], Węglowski et al. [15], and Heidarzadeh et al. [16]; nonetheless, there are no models correlating the tool geometry and process parameters with the final grain size observed in the material after FSP treatment. This is a serious challenge because of the variable thermomechanical conditions and different mechanisms of microstructure evolution. The use of FSP to improve the coarse-grained microstructure of castings in selected areas that are exposed to cyclic stress may contribute to increasing the fatigue resistance. The application of FSP to casting alloys results in homogenization and refinement of the microstructure, the removal of porosity, improvement in the mechanical properties, and increased fatigue strength. Furthermore, in materials after FSP an increase in abrasive wear resistance was found. Nakata et al. [17] investigated the influence of the multi-pass FSP technique on the mechanical properties of a die cast ADC12 aluminium alloy. The obtained results proved that the hardness after modification is about 20 HV higher than that of the base metal. Additionally, the stirring action reduced the porosity and refined large second-phase particles, reducing both their average size and aspect ratios, which have a positive effect on

the tensile strength. Sharma et al. [18] studied the effect of friction stirring on the fatigue behaviour of the A356 alloy. The modification by FSP resulted in significant refinement and uniform distribution of the Si particles in the aluminium matrix, as well as the elimination of porosity. This results in improvement of the fatigue stress threshold > 80% in the stirring area of the FSP sample.

The results of the studies by Ma et al. published in [19] proved that modification by FSP carried out on the A356 aluminium alloy and AZ91 magnesium alloy resulted in a increase in the mechanical properties by the breaking up of coarse dendrites and secondary phases and refinement of matrix grains, as well as the dissolution of precipitates and elimination of porosity. Additionally, the authors noted that this treatment method is ideal for foundry alloys containing coarse particles of secondary phases. Similar results of microstructure studies after FSP of the casting surface of the A356 alloy were also obtained by Reddy and Rao [20]. The refinement and change of the morphology of thick acicular Si particles, as well as their even distribution in the matrix contributed to an increase in hardness and a reduction in the coefficient of friction and a decrease in abrasive wear of the investigated alloy under technically dry friction conditions. In addition, Alidokht et al. [7] proved that an increase in the rotational speed of the tool during FSP modification resulted in a rise in the wear resistance in dry friction conditions. This phenomenon results from the refinement of the microstructure, and more precisely the load-bearing effect of fine and almost spherical Si particles after FSP, which significantly reduces the shear stresses. By means of FSP, it is possible to eliminate agglomerates of the reinforcing phase in composite materials, which has a beneficial effect on the mechanical properties of these materials. The authors of [21] investigated the influence of SiC particles with the number of passes on the microstructural, mechanical and tribological behaviour of AA6082/SiCp composites. The results obtained by the authors indicated that the wear rate of a three-pass FSP AA6082/SiCp composite exhibited a 1.5-times lower wear rate than that of AA6082. This phenomenon is explained by the authors by the homogeneous distribution of the refined reinforcing SiCp that acted as a barrier to material removal during sliding. Additionally, the increase in the number of passes eliminated the cluster formations of the SiCp reinforcing phase and also reduced the particle size from micro to nano, which have a positive effect on the mechanical properties. Parikh et al. [22] focused on the effect of FSP parameters on the microstructure and selected properties of stir cast aluminium-based metal matrix composites. The results prove that performing FSP on as-cast composites has a beneficial effect on their microstructure and microhardness. The most favourable process parameters were a rotational speed of 270 RPM with a transverse speed of 78 mm/min. Recent

literature reports also indicate the use of the FSP method to produce nanocomposites based on ultrafine-grained (UFG) and coarse-grained (CG) commercially pure Al as the matrix and  $\text{Al}_2\text{O}_3$  nanoparticles as the reinforcement [23]. The main conclusion is that it is possible to prevent grain growth in the stir zone of a UFG material while at the same time improving the mechanical properties of the material by means of reinforcement with nanoparticles. An interesting example of the application of the FSP process to manufacture composite materials is bobbin tool-friction stir processing (BT-FSP). The authors of [24] produced an AA1050/silica fume (SF) composite by this method. In this case as well, enhanced mechanical properties were obtained thanks to the addition of a reinforcing phase; the presence of the SF particles also prevented grain growth in the stirring zone.

Tin Babbits, which are the subject of this study, are classified as casting alloys; their microstructure is most often in the three-phase form:  $\alpha$ ,  $\beta$ ,  $\eta$ , where:  $\alpha$  is a solution of antimony and copper in tin, constituting a soft and ductile matrix;  $\beta$  is angular crystals of the SnSb phase;  $\eta$  is acicular precipitates of the  $\text{Cu}_6\text{Sn}_5$  phase. The properties of bearing alloys are highly dependent on the chemical and structural composition. They are used primarily in the energy and electromechanical industries for casting bushings due to, among others, their good tribological properties, resistance to load changes, and good corrosion resistance [25, 26]. In the literature on tin Babbits, information can be found on modification of the microstructure/surface of these alloys to improve the functional properties, in particular the tribological properties. The decisive factor in improving the performance properties of bearing alloys is the refinement and even distribution of hard bearing phases in the soft matrix. Previous research on bearing alloys has focused mainly on improving their mechanical and tribological properties and included, among others: (1) modification of the microstructure using alloying additives [27, 28], improving heat and thermo-plastic treatment processes [29], controlling the rate of crystallization [30, 31] by the choice of manufacturing technology or (2) surface treatment by various techniques [32, 33]. In addition, the scientific base of publications on microstructure refinement as a result of FSP is systematically growing with regard to an increasing number of materials, including casting alloys.

In the literature on bearing alloys, there is no information on attempts to implement FSP to change/modify the phase morphology and possible improvement of the mechanical properties, in particular the tribological properties of these alloys. The authors of the study conducted research on improvement of the properties of these alloys by heat treatment. Bearing in mind the results of the works presented by the authors on the modification of casting alloys by means of FSP, as well as trends in the design of

the microstructure and properties of bearing alloys, the authors of this paper attempted to use the FSP method to modify the microstructure of the tin Babbitt. The results of the research in this area have been partially published by Authors in [34–36] and they prove the refinement of the microstructure, including hard intermetallic phases, as well as the improvement in the mechanical properties, in particular the abrasion resistance of these alloys. The research results presented in the article focus on temperature changes during the process with the Triflute pin.

## 2 Materials and methods

The material to be studied was the tin-based casting alloy SnSb11Cu6. The alloy was poured into cast iron moulds and then cooled in air. The chemical composition of the studied alloy is presented in Table 1. The yield point of the alloy is:  $R_{p0.2} = 61$  MPa, tensile strength  $R_m = 88$  MPa, and elongation  $A = 6\%$  (at the temperature of 20 °C) [37].

**Table 1** Chemical composition of investigated alloy, wt%

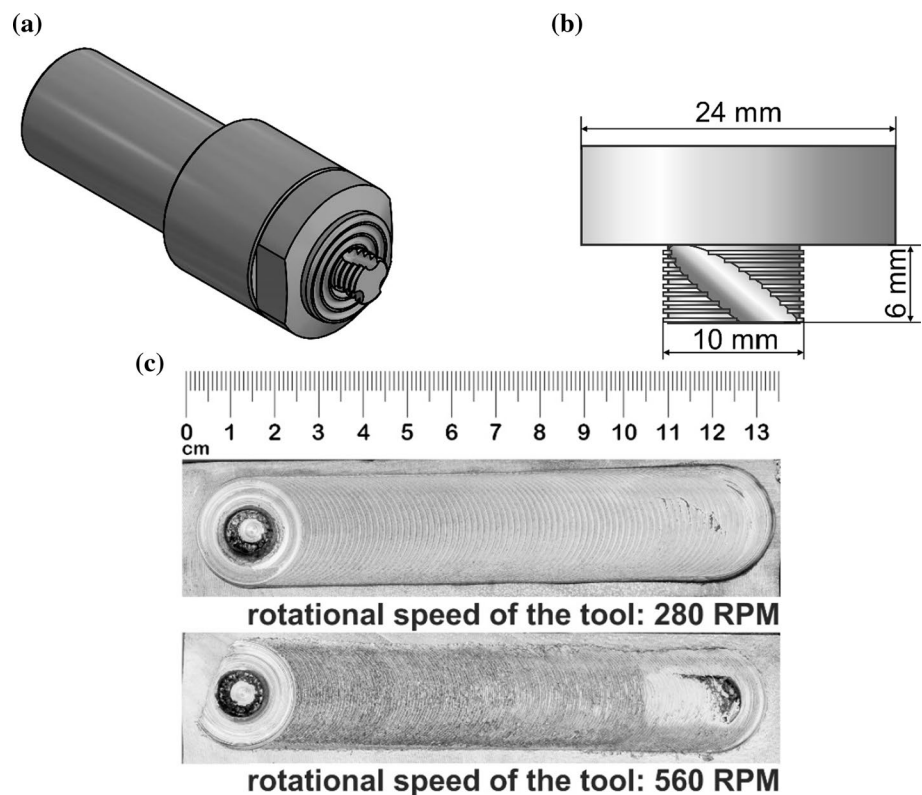
Alloy grade	Chemical composition, wt%			
SnSb11Cu6	Sn	Sb	Cu	Pb
	82.1	11.1	6.5	0.3

FSP modification was carried out on a welding stand built on an FYF32JU2 vertical milling machine. The process was carried out using a Triflute pin (Fig. 1a, b). Among others, the grooves on the pin increase the heat generated by increasing the contact surface between the pin and the workpiece, resulting in a more efficient process. The tool is made of high-speed steel HS 6-5-2. FSP was conducted using two rotational speeds of the tool: 280 and 560 RPM and a constant linear speed of 355 mm/min.

The surface of the face after FSP modification showed traces of tool progress in the form of "semicircles", characteristic for this method of machining (Fig. 1c). The distance between the semicircles decreases as the rotational speed of the tool increases. Under modification conditions at the higher rotational speed of 560 RPM, discontinuities occurred on the surface, but they were located only on the surface layer, and it is easy to remove, which allows the exposure of a material with very good properties compared to the reference material.

Examination of the microstructure of the samples before and after FSP modification was performed by means of light microscopy (OLYMPUS GX51 microscope) and scanning electron microscopy along with EDS analysis of the chemical composition in micro-areas (Hitachi SU 70 microscope). Additionally, the phase composition was analysed utilising a BRUKER X-ray diffractometer with a  $\text{Co } K\alpha = 0.179$  nm (1.79 Å) cobalt lamp. Data were

**Fig. 1** Triflute tool. **a** Triflute tool used for modification, **b** tool dimensions, and **c** photo of samples after FSP modification process





compiled using the Powder Diffraction File database developed and published by ICDD (The International Centre for Diffraction Data). Hardness measurements were made by means of the Brinell method according to the PN-EN ISO 6506-1 standard with a hardness tester by Innovatest; a tungsten carbide ball with a diameter of 2.5 mm and a load of 31.25 kG were employed.

Analyses using the electron backscatter diffraction (EBSD) method were carried utilising a Hitachi S-3400N scanning electron microscope and detector with dedicated software made by HKL. An accelerating voltage of 20 kV was used for the tests. The sample was tilted at an angle of  $70^\circ$  at a distance of approximately 20 mm from the column. The electron backscatter diffraction analysis was performed to obtain maps of the crystal lattice orientation distribution on the surface of the test sample with a  $0.5\ \mu\text{m}$  step at the magnification of  $200\times$  and  $0.15\ \mu\text{m}$  step at the magnification of  $1000\times$ . The colours of the solved orientations were assigned according to the basic IPF triangle notation. The results are presented in the form of a map of the crystallographic orientation distribution on the sample surface.

Additionally, measurements of the temperature directly on the modified surface by means of a thermal imaging camera and the temperature in the modified zone with a thermocouple system (placed in selected areas of the stir zone) were performed. The  $k$ -type thermocouples were located 7 and 15 mm from the centre of the FSP zone, at a depth of 2.7 and 2.3 mm, respectively. Figure 2 shows the location of the 12 thermocouples in the process zone.

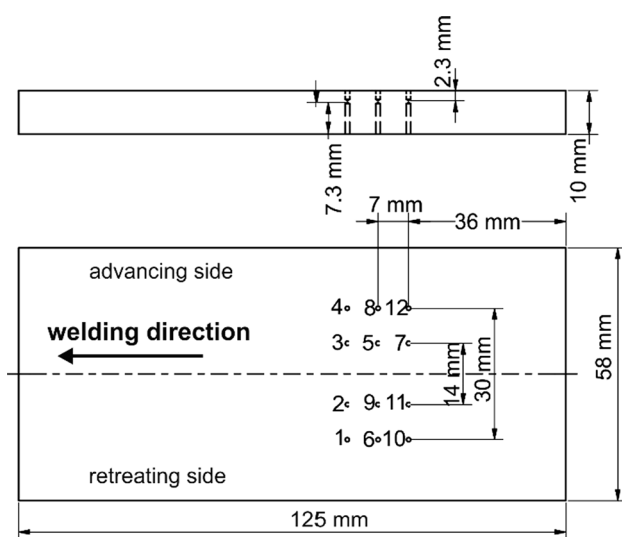


**Fig. 2** Diagram of thermocouple distribution in sample modified by FSP

### 3 Results and discussion

The results of examining the microstructure of the as-cast SnSb11Cu6 alloy (before the modification of the FSP) are presented in Fig. 3, while Figs. 4 and 5 show pictures of the microstructure after modification of the surface layer by FSP with a Triflute pin. Moreover, Fig. 6 presents the results of the X-ray phase analysis of the alloy before and after FSP modification. The microstructure of the investigated alloy before modification consists of large diamond-shaped and cubic precipitates with a size in the range of  $50\text{--}400\ \mu\text{m}$  and the stoichiometry corresponding to the SnSb phase (Fig. 3b, point 1). Furthermore, there are numerous acicular and globular-shaped precipitates in the alloy microstructure with  $\text{Cu}_6\text{Sn}_5$  phase stoichiometry (Fig. 3b, pts. 3 and 4). Observations of the alloy microstructure after FSP modification depending on the rotational speed of the tool (Figs. 4, 5) revealed no discontinuities or pores, nor a distinct characteristic nucleus. The shape and structure of SZ changed as the rotational speed of the Triflute increased. The depth of SZ hardly changes with the increment in the rotational speed and amounts to approx. 7 mm for each variant. Likewise, the width of this zone, measured at the middle and lower levels, is constant at approx. 10 mm. Only the width of the zone in the upper level changes, which is influenced by the effect of the tool shoulder. For SZ after FSP treatment at 280 RPM, the width measured at the top of the zone is 15 mm, while for the FSP sample with 560 RPM rotational speed, there is hardly any visible effect of the shoulder on the microstructure; the measured width of the stir zone is 10 mm. In the microstructure of the alloy modified at the speed of 280 RPM, no clear boundary was noticed on the advancing side or on the retreating side (Fig. 4), whereas in the material processed at the rotational speed of 560 RPM, there is a clear boundary that separates the area of fine grains from the area of larger grains (Fig. 5). A similar phenomenon occurs in the lower transition zone. The occurrence of a clear boundary between the treated zone and the initial material is not a desirable phenomenon, as it may contribute to the formation of various defects in the material, such as spalling.

The results of the microstructure observations presented in Figs. 4 and 5 indicate a change in the morphology of the phases present in the studied alloy after FSP. Both SnSb and  $\text{Cu}_6\text{Sn}_5$  precipitates were significantly refined, and the shape changed to a more regular, close to globular one. It was found that the acicular form of the  $\text{Cu}_6\text{Sn}_5$  phase was completely eliminated in favour of the globular shape. Strong refinement of the tin-rich matrix was also noted in the FSP-modified area. In this case, fine and equiaxed recrystallized tin-rich grains of approx.  $5\text{--}30\ \mu\text{m}$

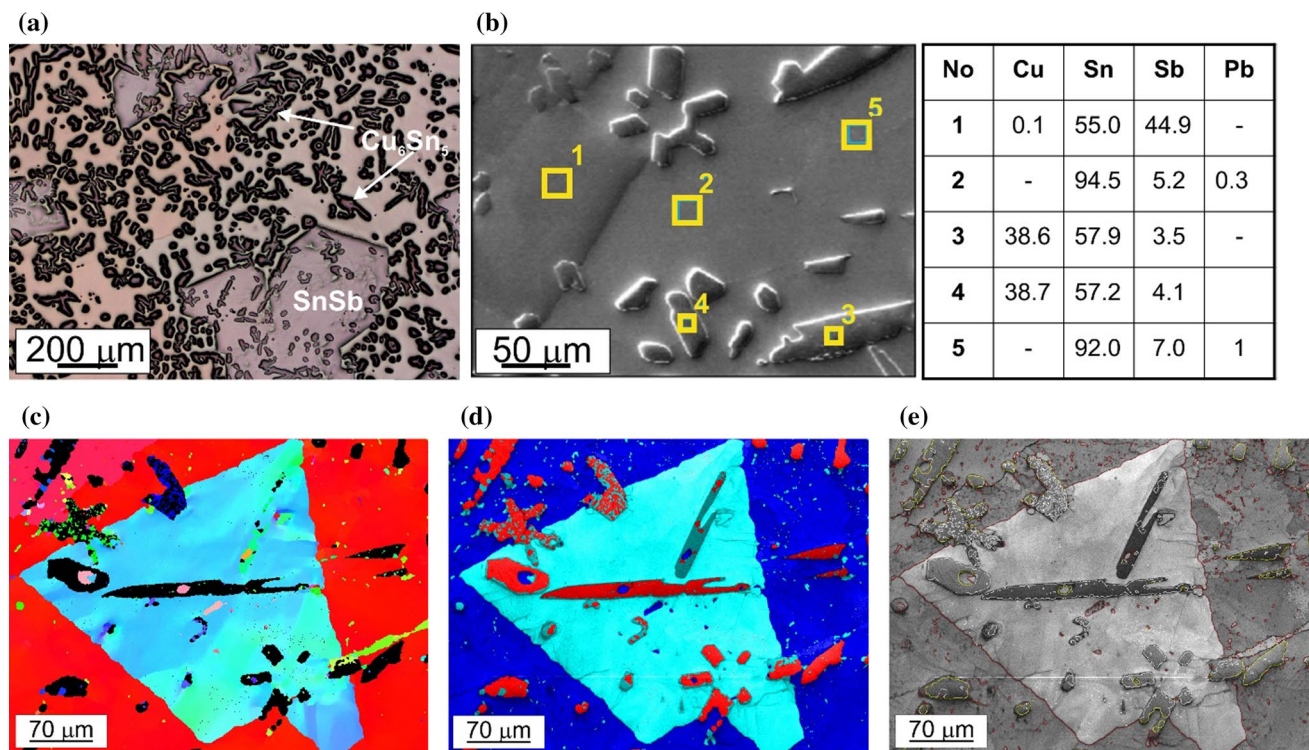


**Fig. 3** Microstructure of SnSbCu alloy in initial state after casting: **a** micrograph taken using light microscope, **b** microstructure and point analysis results; **c–e** EBSD analysis results of initial sample, mag.

200× (**c**—based orientation+pattern quality map (IPF), **d**—band contrast (BC), **e**—band contrast and lattice coordinate (LC))

in size were formed in the stir zone. The results of the X-ray phase analysis (Fig. 6) did not reveal the formation of new phases after the FSP treatment, but it can be seen that some of the Pb peaks and the  $\text{Cu}_6\text{Sn}_5$  phases are more intense, which confirms the refinement of this phase during the FSP treatment. Reduction of the size of the microstructure components of the investigated alloy, as well as their homogenization, are favourable from the point of view of the mechanical properties, including the tribological properties, which is confirmed by the authors' previous research [34, 35].

The parameters of FSP have a decisive influence on the quality of the produced microstructure [38, 39]. The state of knowledge regarding the phenomena occurring during FSP is not yet fully known, which makes it difficult to select optimal parameters for various alloys. The research presented in the paper shows a change in the structure of the FSP zone with the increase in the rotational speed of the tool.

The results of the research by Hamilton et al. [11, 12] prove that the temperature distribution in the FSP process zone is not uniform and changes in a gradient manner. The highest temperature occurs on the upper surface of the process zone, which is related to the heat generated by the tool shoulder. The obtained results of measurements by

means of a thermal imaging camera and thermocouples confirmed the inhomogeneous temperature distribution in the process zone (Figs. 7, 8; Table 2).

Temperature measurements utilising the thermal imaging camera proved that an increase in the rotational speed causes growth in the temperature on the alloy surface. It is especially visible on the retreating side, where at the tool rotational speed of 280 RPM, the average temperature measured on the surface was approx. 208 °C, while for machining at 560 RPM, the temperature increased to 236 °C (Table 2). It is worth noting that at the lower rotational speed, the advancing side was warmer than the retreating side; the opposite was true for 560 RPM. Likewise, the thermocouple measurements revealed higher temperatures on the retreating side compared to the advancing side at higher rotational speeds. When employing the low rotational speed of the tool (280 RPM), the temperature distribution is very similar on both sides and is in the range of 80–100 °C in HAZ (Fig. 8a) and 90–105 °C in TMAZ (under the shoulder, Fig. 8b). For the modification with the rotational speed of 560 RPM, the recorded temperature values in HAZ rose slightly on the retreating side, reaching a value in the range of 90–110 °C (Fig. 8c), while in TMAZ, the temperature increment is clear; the highest temperature was measured by thermocouple No. 11—approx. 160 °C, and then, there



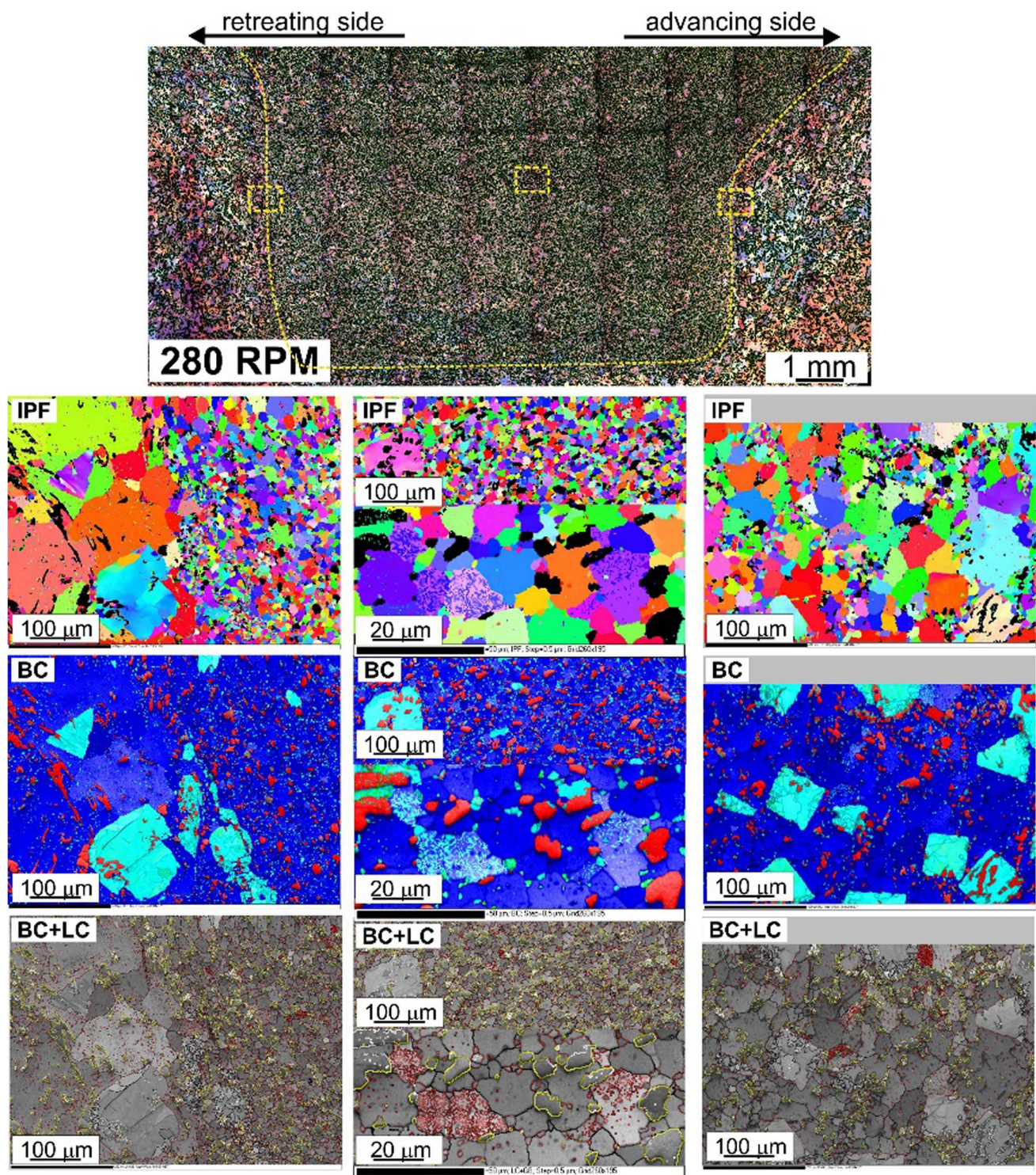


**Fig. 4** Microstructure of SnSbCu alloy after FSP modification at 280 RPM; EBSD analysis results from marked places are included in the figure

is a sharp drop in temperature to 100 °C (after approx. 3 s), after which the material cools down more slowly (Fig. 8d).

The main contributor to the generation of heat is the friction between the tool and the material being modified. The shoulder, in contact with the surface of the modified

element, exerts pressure on the treated surface, generates heat as a result of friction, and causes plastic deformation in a relatively thin layer (directly under the shoulder surface). As the rotational speed increases, the share of thermal energy from the shoulder decreases in favour of the energy



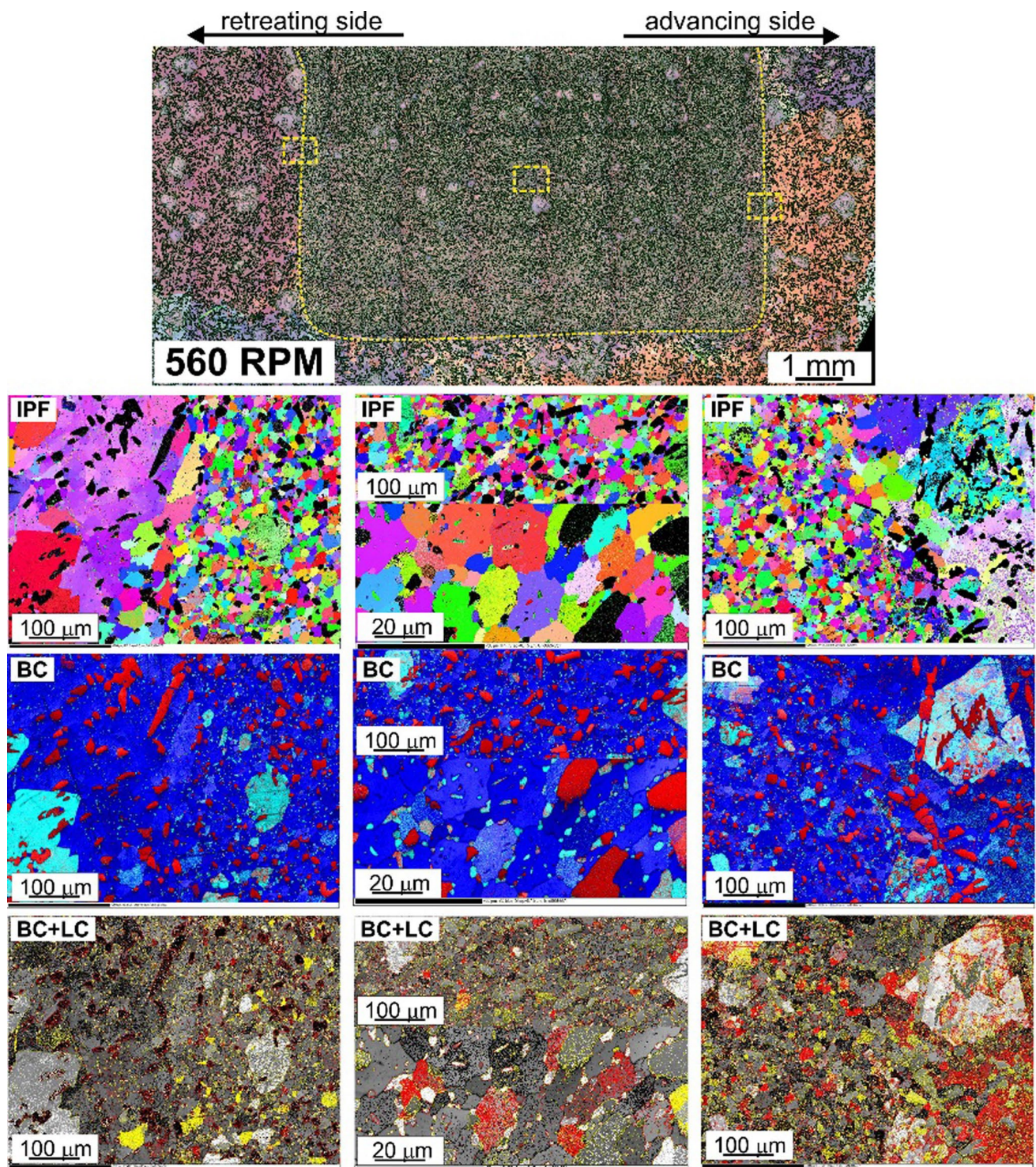


**Fig. 5** Microstructure of SnSbCu alloy after FSP modification at 560 RPM; EBSD analysis results from marked places are included in the figure

supplied from the pin. The results of numerical simulations presented by the authors of [12, 13] indicate that the advancing side is usually the hotter side of the FSP zone, as a consequence of the higher level of stress in relation to the retreating side in the modified material. This is related to the

consistent direction of rotation and travel of the tool on the advancing side, while on the retreating side, these directions are the opposite. In the case of a constant linear speed, as the rotational speed increases, the maximum temperature distribution moves from the advancing side towards the



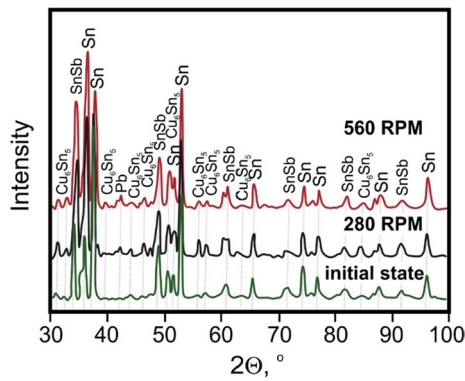


**Fig. 6** X-ray diffraction pattern of SnSbCu alloy for initial material and after FSP modification

retreating side, which may explain the higher temperature on the retreating side in the studied material, during FSP carried out at the rotational speed of 560 RPM.

The results recorded by the thermocouples proved that the  $T_f$  of the SnSbCu alloy was not exceeded in the process zone; because the range of  $0.4\text{--}0.7 T_f$  was reached in the TMAZ zone, a temperature of  $>0.7 T_f$  can be expected in SZ. FSP generates a significant increase in temperature due to frictional forces, intense plastic deformation, and material flow caused by the movement of the tool, thus promoting dynamic recrystallization (DRX) in the stir zone (SZ). The research results presented by Zainulabdeen et al. [40] prove the dynamic recrystallization of bearing alloys on a tin matrix during downward extrusion. In turn, Sadykov [25] writes that recrystallization will take place at room temperature after inflicting 20% cold deformation. Owing to the favourable conditions for dynamic recrystallization in SZ, re-precipitation of the second phase may take place during cooling—after the passage of the tool. In addition,

it was observed that some of the SnSb phase precipitates have cracks on the surface, which indicates their breaking (mechanically) into smaller particles by the Triflute tool during friction stir processing. Moreover, the increase in the rotational speed of the tool favoured a more even distribution of SnSb and  $\text{Cu}_6\text{Sn}_5$  phases in relation to the distribution in the starting material. Additionally, the presented thermovision results suggest that the temperature may be exceeded, the studied alloys may melt, and local melting points may appear on the material surface, especially along the central axis of the process zone, where both the pin and the shoulder contribute to heat generation, and the temperature reached the average value of approx.  $290^\circ\text{C}$  (Table 2).

The melting range of the tested SnSbCu alloy is within the temperature range of  $240\text{--}370^\circ\text{C}$  [41]. Figure 9 shows the DTA curves of the melting and solidification processes of the investigated alloy, while the solidus and liquidus temperatures determined in the DTA test are presented in Table 3. The cooling curves of the examined alloy show three distinct peaks at the reaction temperature, successively:  $376$ ,  $262$ , and  $234^\circ\text{C}$ . During cooling, the first peak is associated with the  $\eta$  phase crystal precipitate ( $\text{Cu}_6\text{Sn}_5$ ) at  $376^\circ\text{C}$ , the second one with  $\beta$  phase (SnSb) crystallization at  $262^\circ\text{C}$ , and the third one corresponds to the solid solution  $\alpha$  phase precipitate (Sn)—the matrix at  $234^\circ\text{C}$ . In turn, the heating curves revealed additionally small peaks at the temperatures of about  $350^\circ\text{C}$  and  $416^\circ\text{C}$ . The occurrence of these peaks may be related to the changes taking place in the solid phase and the appearance of an additional phases  $\delta$  ( $350^\circ\text{C}$ ) and  $\epsilon$  ( $415^\circ\text{C}$ ) [42]. The results of the X-ray phase analysis do not confirm this; however, it may be related to the too small proportion of these phases in the alloy.

The refinement of the precipitates and their even distribution in the matrix translated into an increase in the

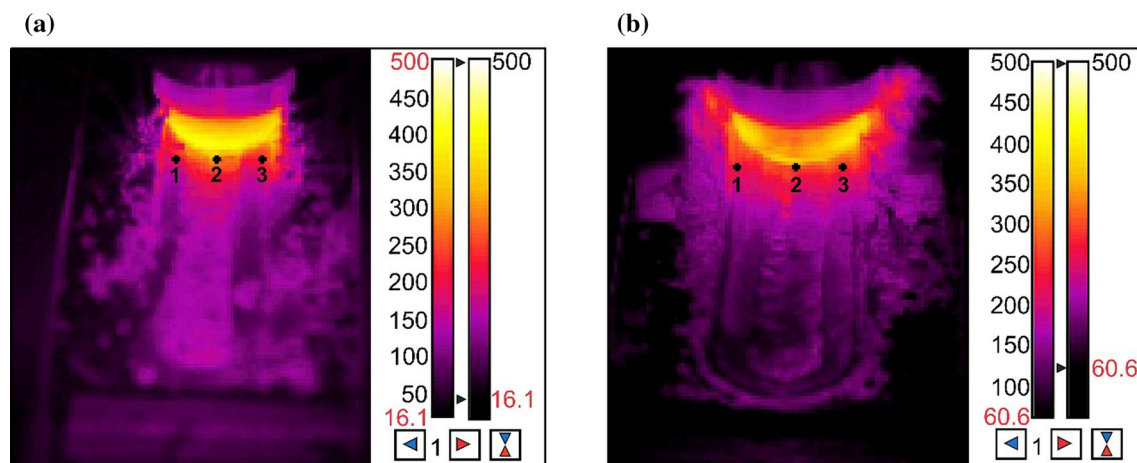


**Fig. 7** Thermogram of modified SnSbCu alloy surface in FSP process; **a** 280 RPM and **b** 560 RPM

**Fig. 8** Material temperature in process zone measured during FSP of SnSbCu alloy at different rotational speeds of Triflute tool: **a** and **b** 280 RPM, **c** and **d** 560 RPM

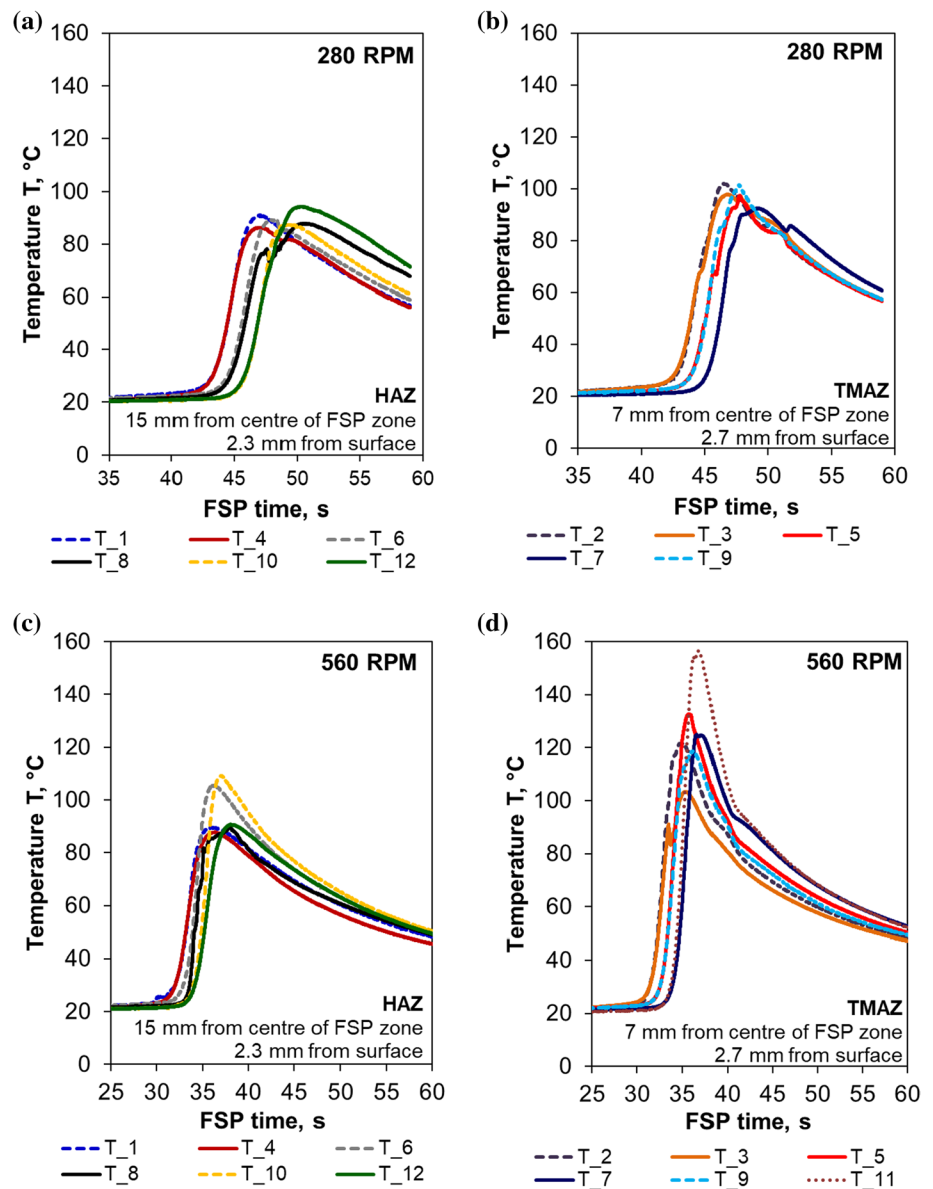


**Table 2** Average temperature values measured on SnSbCu alloy face measured during tool pass in FSP process

Temperature $T$ , °C		
Variant	280 RPM	560 RPM
Advancing side (pt. 1)	$220 \pm 18$	$226 \pm 23$
Middle of process zone (pt. 2)	$289 \pm 29$	$290 \pm 19$
Retreating (pt. 3)	$208 \pm 14$	$236 \pm 14$

Brinell hardness in the case of the investigated alloy. The hardness of the alloy after modification by FSP at the speed of 560 RPM increased by 12% compared to the starting material and was, respectively, 24 HB for the starting material, 25 HB for the material after the processing at 280

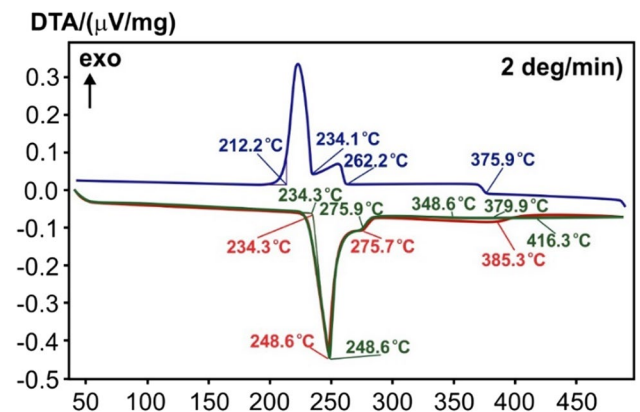


**Fig. 9** DTA curves of melting and solidification processes of SnSbCu alloy



**Table 3** Melting range of investigated alloy determined using DTA heating and cooling curves

Solidus		Liquidus	
Heating, $T_{\text{onset}}$ (°C)	Cooling, $T_{\text{endset}}$ (°C)	Heating, $T_{\text{onset}}$ (°C)	Cooling, $T_{\text{endset}}$ (°C)
234.3	234.1	416.3	375.9

RPM, and 27 HB for the material after the processing at 560 RPM. The increase in hardness after FSP treatment is mainly determined by the refinement of the precipitates present in the alloy, and the SnSb phase precipitate is of particular importance. It is equally important to homogenize the microstructure. The large precipitates in this phase are characterised by brittle fracture. The finer the particles, the more difficult their brittle fracture becomes and the ductile fracture proportion increases. As a result of the FSP treatment of the alloy, the average particle area of both the SnSb and  $\text{Cu}_6\text{Sn}_5$  phases is ten times smaller compared to the size of these precipitates in the cast alloy, and the distance between the precipitates also decreased [34].

## 4 Conclusions

On the basis of the conducted experimental research, the following conclusions were formulated:

1. The use FSP for the surface treatment of the SnSbCu alloy results in significant grain refinement and hard phases. The microstructure in the stir zone is shaped by the dynamic recrystallization (DRX) process and consists of almost equiaxed tin-rich matrix grains with a size of approx. 5–30  $\mu\text{m}$  and fine particles of SnSb phases and  $\text{Cu}_6\text{Sn}_5$ .
2. The temperature distribution in the FSP zone is not uniform and changes in a gradient manner. The highest temperature is at the top of the process zone, which is related to the heat generated by the tool shoulder. Also, an increase in the rotational speed of the tool causes an increase in the temperature on the alloy surface. With the tool rotational speed of 280 RPM, the average temperature measured on the surface of the alloy was approx. 208 °C, while for machining at 560 RPM, the temperature increased to 236 °C.
3. The tool in the FSP process causes the advantageous breakdown of the SnSb phase precipitates into smaller particles and an even distribution of SnSb and  $\text{Cu}_6\text{Sn}_5$  phases in relation to the initial material.
4. The refinement of the precipitates and their uniform distribution in the matrix of the modified tin alloy increased the Brinell hardness in relation to the initial

material (24 HB), respectively, 25 HB for the tool rotational speed of 280 RPM and 27 HB for the tool rotational speed of 560 RPM.

5. The cooling curves show three distinct peaks at the reaction temperature, successively at 376, 262, and 234 °C. During cooling, the first peak is associated with the  $\eta$  phase crystal precipitate ( $\text{Cu}_6\text{Sn}_5$ ) at 376 °C, and the second with crystallization of the  $\beta$  phase (SnSb) at 262 °C, while the third one corresponds to the  $\alpha$  phase (Sn) solid solution precipitate at the temperature of 234 °C.

**Acknowledgements** The authors would like to acknowledge prof. Bogusław Onderka (UST-AGH, Faculty of Non-Ferrous Metals, Poland) for support concerning DTA investigations.

**Author contributions** Conceptualization: B.L.-M.; methodology: B.L.-M., A.W., and M.M.; investigation: B.L.-M., J.H.-W., A.W., M.P.-N., and M.M.; writing—original draft preparation: B.L.-M.; writing—review and editing: B.L.-M., J.H.-W., A.W., and M.M.; visualization: B.L.-M. and J.H.-W.; Resources: B.L.-M.; Supervision: B.L.-M. All authors have read and agreed to the published version of the manuscript.

**Funding** Partial financial support was received from Polish State Committee for Scientific Research, under Grant No. 16.16.180.006. The authors have no financial or proprietary interests in any material discussed in this article.

**Availability of data and materials** The authors confirm that the data supporting the findings of this study are available within the article [and/or] its supplementary materials.

## Declarations

**Conflict of interest** The authors declared no potential conflicts of interest with respect to the research, authorship, and/or publication of this article.

**Ethical approval** This article does not contain any studies with human participants or animals performed by any of the authors.

**Open Access** This article is licensed under a Creative Commons Attribution 4.0 International License, which permits use, sharing, adaptation, distribution and reproduction in any medium or format, as long as you give appropriate credit to the original author(s) and the source, provide a link to the Creative Commons licence, and indicate if changes were made. The images or other third party material in this article are included in the article's Creative Commons licence, unless indicated otherwise in a credit line to the material. If material is not included in the article's Creative Commons licence and your intended use is not permitted by statutory regulation or exceeds the permitted use, you will need to obtain permission directly from the copyright holder. To view a copy of this licence, visit <http://creativecommons.org/licenses/by/4.0/>.

## References

- Mishra RS, Mahoney MW, McFaden SX, Mara NA, Mukherjee AK. High strain rate superplasticity in a friction stir processed 7075 Al alloy. *Scr Mater*. 2000. [https://doi.org/10.1016/S1359-6462\(99\)00329-2](https://doi.org/10.1016/S1359-6462(99)00329-2).
- Thomas WM. Friction stir butt welding. GB patent 9125978, 6.12.1991, International patent application PCT/GB92/02203
- Thomas WM, Nicholas ED, Needham JC, Murch MG, Temple-Smith P, Dawes CJ. Improvements relating to friction welding. Patent European Patent Specification 0 615 480 B1
- Givi MK, Asadi P. *Advances in friction stir welding and processing*. Amsterdam: Woodhead Publishing; 2014.
- Węglowski MS. Experimental study and response surface methodology for investigation of FSP process. *Arch Mech Eng*. 2014. <https://doi.org/10.2478/meceng-2014-0031>.
- Desai AM, Khatri BC, Patel V, Rana H. Friction stir welding of AZ31 magnesium alloy: a review. *Mater Today Proc*. 2021. <https://doi.org/10.1016/j.matpr.2021.03.082>.
- Alidokht SA, Abdollah-Zadeh A, Soleymani S, Saeid T, Assadi H. Evaluation of microstructure and wear behavior of friction stir processed cast aluminum alloy. *Mater Charact*. 2012. <https://doi.org/10.1016/j.matchar.2011.11.007>.
- Li K, Liu X, Zhao Y. Research status and prospect of friction stir processing technology. *Coatings*. 2019. <https://doi.org/10.3390/coatings9020129>.
- Shercliff HR, Colegrove PA. Modelling of friction stir welding. *Math Model Weld Phenom*. 2002. <https://doi.org/10.17863/CAM.14008>.
- Węglowski MS, Pietras A, Dymek S, Hamilton C. Characterization of friction stir processing applied for modification of surface microstructure in a cast aluminium alloy. In: *Proceedings of the 14th International Conference Metalforming*. 2012. p 587–590.
- Hamilton C, Kopyściński M, Senkov O, et al. A coupled thermal/material flow model of friction stir welding applied to Sc-modified aluminum alloys. *Metall Mater Trans A*. 2013. <https://doi.org/10.1007/s11661-012-1512-y>.
- Hamilton C, Węglowski MS, Dymek S. A simulation of friction-stir processing for temperature and material flow. *Metall Mater Trans B*. 2015. <https://doi.org/10.1007/s11663-015-0340-z>.
- Węglowski MS, Sedek P, Hamilton C. Experimental analysis of residual stress in friction stir processed cast AlSi9Mg aluminium alloy. *KEM*. 2016. <https://doi.org/10.4028/www.scientific.net/kem.682.18>.
- Ma Z. Friction stir processing technology: a review. *Metall Mater Trans A*. 2008. <https://doi.org/10.1007/s11661-007-9459-0>.
- Węglowski MS. Friction stir processing—state of the art. *Arch Civil Mech Eng*. 2018. <https://doi.org/10.1016/j.acme.2017.06.002>.
- Heidarzadeh A, Mironov S, Kaibyshev R, Çam G, Simar A, Gerlich A, Khodabakhshi F, Mostafaei A, Field DP, Robson JD, Deschamps A, Withers PJ. Friction stir welding/processing of metals and alloys: a comprehensive review on microstructural evolution. *Prog Mater Sci*. 2020. <https://doi.org/10.1016/j.pmatsci.2020.100752>.
- Nakata K, Kim YG, Fujii H, Tsumura T, Komazaki T. Improvement of mechanical properties of aluminum die casting alloy by multi-pass friction stir processing. *Mater Sci Eng A*. 2006. <https://doi.org/10.1016/j.msea.2006.07.150>.
- Sharma SR, Ma ZY, Mishra RS. Effect of friction stir processing on fatigue behavior of A356 alloy. *Scr Mater*. 2004. <https://doi.org/10.1016/j.scriptamat.2004.04.014>.
- Ma ZY, Pilchak AL, Juhas MC, Williams JC. Microstructural refinement and property enhancement of cast light alloys via friction stir processing. *Scr Mater*. 2008. <https://doi.org/10.1016/j.scriptamat.2007.09.062>.
- Reddy GM, Rao KS. Enhancement of wear and corrosion resistance of cast A356 aluminium alloy using friction stir processing. *Trans Indian Inst Met*. 2010. <https://doi.org/10.1007/s12666-010-0121-y>.
- Sivanesh PM, Elaya PA, Arulvel S. Development of multi-pass processed AA6082/SiCp surface composite using friction stir processing and its mechanical and tribology characterization. *Surf Coat Technol*. 2020. <https://doi.org/10.1016/j.surfcoat.2020.125900>.
- Parikh VK, Badgujar AD, Ghetiya ND. Effect of Friction stir processing parameters on microstructure and microhardness of aluminium based Metal matrix composites. *Mater Today Proc*. 2022. <https://doi.org/10.1016/j.matpr.2022.03.386>.
- Orłowska M, Pixner F, Hütter A, Enzinger N, Olejnik L, Lewandowska M. Manufacturing of coarse and ultrafine-grained aluminum matrix composites reinforced with Al<sub>2</sub>O<sub>3</sub> nanoparticles via friction stir processing. *J Manuf Process*. 2022. <https://doi.org/10.1016/j.jmapro.2022.06.011>.
- Ahmed MMZ, Selemam MME, Eid RG, Zawrah MF. Production of AA1050/silica fume composite by bobbin tool-friction stir processing: microstructure, composition and mechanical properties. *CIRP J Manuf Sci Technol*. 2022. <https://doi.org/10.1016/j.cirpj.2022.07.002>.
- Sadykov FA, Barykin NP, Valeev IS, Danilenko VN. Influence of the structural state on mechanical behavior of tin Babbitt. *J Mater Eng Perform*. 2003. <https://doi.org/10.1361/105994903770343448>.
- Leszczyńska-Madej B, Madej M, Hrabia-Wiśnios J. Effect of chemical composition on the microstructure and tribological properties of Sn-based alloys. *J Mater Eng Perform*. 2019. <https://doi.org/10.1007/s11665-019-04154-4>.
- Sotomi I, Tamura K, Goshima T. Effect of amount of antimony on sliding wear resistance of white metal. *Tribol Int*. 2010. <https://doi.org/10.1016/j.triboint.2009.12.047>.
- Zhao J, Sun K, Liang G, Xu C, Zhao J, Xue F, Zhou J. Effect of Zn additions on the microstructure and mechanical properties of Sn-Babbitt alloys fabricated by arc deposition. *J Market Res*. 2021. <https://doi.org/10.1016/j.jmrt.2021.11.097>.
- Barykin NP, Fazlyakhmetov RF, Valeeva AK. Effect of the structure of Babbitt B83 on the intensity of wear of tribo couplings. *Met Sci Heat Treat*. 2006. <https://doi.org/10.1007/s11041-006-0050-x>.
- Potekhin BA, Ilyushin VV, Khristolyubo AS. Effect of casting methods on the structure and properties of tin Babbitt. *Metal Sci Heat Treat*. 2009. <https://doi.org/10.1007/s11041-009-9181-1>.
- Gajmal SS, Jijabai V. An investigation on wear behaviour of ASTM B23 tin-based Babbitt alloy developed through microwave-assisted casting. *Int J Metalcast*. 2022. <https://doi.org/10.1007/s40962-021-00721-5>.
- Dong YN, Tong Z, Li X, Wang W. Effect of laser remelting on tribological properties of Babbitt alloy. *Mater Res Express*. 2019. <https://doi.org/10.1088/2053-1591/ab308d>.
- Zhao X, Lai R, Hai X. A study on the microstructures and properties of selective laser melted Babbitt metals. *J Mater Eng Perform*. 2019. <https://doi.org/10.1007/s11665-019-04332-4>.
- Leszczyńska-Madej B, Madej M, Hrabia-Wiśnios J, Węglowska A. Effects of the processing parameters of friction stir processing on the microstructure, hardness and tribological properties of SnSbCu bearing alloy. *Materials*. 2020. <https://doi.org/10.3390/ma13245826>.
- Madej M, Leszczyńska-Madej B, Hrabia-Wiśnios J, Węglowska A. Effect of FSP on tribological properties of grade B89 tin Babbitt. *Materials*. 2021. <https://doi.org/10.3390/ma14102627>.



36. Hrabia-Wiśnios J, Leszczyńska-Madej B, Madej M, Węglowska A. Characterization of microstructure and selected properties of SnSbCu alloy after FSP. *Int J Adv Manuf Technol*. 2021. <https://doi.org/10.1007/s00170-021-07781-1>.
37. PN-ISO 4381:1997
38. Leal RM, Galvão I, Loureiro A, et al. Effect of friction stir processing parameters on the microstructural and electrical properties of copper. *Int J Adv Manuf Technol*. 2015. <https://doi.org/10.1007/s00170-015-7141-z>.
39. Garcia-Bernal MA, Mishra RS, Verma R, Hernandez-Silva D. Influence of friction stir processing tool design on microstructure and superplastic behavior of Al–Mg alloys. *Mater Sci Eng A*. 2016. <https://doi.org/10.1016/j.msea.2016.05.115>.
40. Zainulabdeen AA, Hashim FA, Assi SH. Mechanical properties of Tin-based Babbitt alloy using the direct extrusion technique. *ICSET Mater Sci Eng*. 2019. <https://doi.org/10.1088/1757-899X/518/3/032031>.
41. PN-82/H-87111
42. Predel B. Phase equilibria, crystallographic and thermodynamic data of binary alloys. In: Predel B, editor. *Numerical data and functional relationships in science and technology*. Berlin: Springer; 2012.

**Publisher's Note** Springer Nature remains neutral with regard to jurisdictional claims in published maps and institutional affiliations.